Bulk and surface processes in low-energy-electron-induced decomposition of CaF_2

R. Bennewitz,* D. Smith, and M. Reichling†
Fachbereich Physik, Freie Universität Berlin, Arnimallee 14, 14195 Berlin, Germany
(Received 9 June 1998)

The irradiation of CaF_2 with low-energy (typically 1 keV) electrons results in a decomposition of the crystal and the formation of metallic clusters on its surface, and in a near-surface layer. In this paper we describe the formation of surface clusters and their typical shapes and transformations they undergo in an ultrahigh-vacuum environment. From the evidence found in a variety of experiments, we conclude that surface metallization is strongly related to diffusive transport of irradiation-induced defects. We can coherently explain experimental results presented here, and earlier observations, by assuming that both the conversion of primarily created *F* and *H* center defects into charged V_k and *I* centers, as well as their electric-field-induced diffusion, are controlled by the electron irradiation. Fluorine diffusion into the bulk leads to the formation of subsurface fluorine gas bubbles appearing as micron-sized surface elevations in scanning force microscopy images. For the initial stages of metal cluster formation on the (111) surface, we observe ordering phenomena indicating an epitaxial growth. Due to oxidation the surface topography changes when metal clusters are subjected to a residual gas atmosphere of 1×10^{-9} mbar for more than one day. [S0163-1829(99)05508-3]

I. INTRODUCTION

There is technological interest in the electron-induced modification of CaF_2 from two points of view: First, insulating layers of CaF_2 can be structured by electron-beam lithography[1] and ''hole drilling'' with high-energy electron beams,[2] processes that may both become important for the use of CaF_2 in microelectronic devices.[3] The second technological impact of electron-induced surface modifications is the improvement of epitaxial growth of GaAs overlayers[4,5] as well as Si overlayers[6] on $CaF_2(111)$, known as electron-beam-assisted molecular-beam epitaxy. To understand these processes, it is important to investigate the initial stages of electron-induced surface modifications, which is one aim of the present paper.

In our previous work, several aspects of low-energy electron-induced decomposition of CaF_2 have already been treated, namely, the penetration depth of primary electrons,[7] the formation of bulk colloids and surface metal clusters,[8] and the electron-stimulated desorption of fluorine.[9]

The penetration depth of primary electrons with an energy E in CaF_2 has been found to obey the equation $L=19\,\mathrm{nm}\times(E/\mathrm{keV})^{1.45}$ by simulating electron trajectories.[7] Here the penetration depth L is defined as the depth where the energy of primary electrons falls below three times the band-gap energy, which is assumed to be the lower limit for electron-hole-pair excitation. A penetration depth of 15 nm results for the energy of 850 eV mostly used in experiments discussed here. The depth of maximum energy loss (two times larger than at the surface) and, therefore, of most effective defect creation is 25% of the penetration depth.

Optical spectroscopy of electron irradiated CaF_2 reveals the development of calcium colloids in the bulk of the crystal.[8] For irradiation with 2.5 keV electrons at room temperature and above, one can expect typical colloid radii between 15 and 30 nm. Colloid formation results from aggregation of *F* centers, a process favored in CaF_2 by the good match between the lattice structure and atomic spacing of calcium metal and the Ca^{2+} sublattice in CaF_2 (see Table I).

An important observation in electron-stimulated desorption studies on CaF_2 relevant for the defect transport studies discussed in this paper is delayed desorption.[9] The delay between the start of irradiation and the maximum of the desorption yield indicates that desorption is fed by diffusion of fluorine from the bulk to the surface. In a simple picture the desorption reaches a maximum when fluorine from a depth corresponding to the depth of maximum defect creation arrives at the surface. For longer irradiation times the desorption yield decreases due to depletion of bulk fluorine, and masking of the surface by metal.

Indirect evidence that diffusive transport is not only thermally activated but stimulated by electron irradiation was found in a scanning force microscopy study of low-energy electron-induced surface metallization on $CaF_2(111)$, where the amount of surface metal was measured as a function of electron irradiation time.[10] Surprisingly, the dependence of metallization on irradiation time was found to be quadratic, and this observation can be explained by assuming diffusive transport of *F* centers from the bulk to the surface where diffusion is activated only during the time of electron irradiation. Such diffusive transport is the dominant process in experiments with a low electron intensity, applied for a longer time of observation and relevant for all measurements presented here. At higher irradiation intensity, however, col-

TABLE I. Physical properties of the Ca compounds discussed. Values are taken from *CRC Handbook of Chemistry and Physics* (CRC Press, Cleveland, 1976).

	Lattice structure	Lattice constant (Å)	Molecular volume (Å^3)
Ca	fcc	5.57	43.2
CaF_2	fcc	5.46	40.8
CaO	bcc	3.83	28.1

loid formation due to fluorine desorption directly from the surface may become important.[10]

In the present paper, we describe bulk and surface processes of the decomposition of CaF_2 single crystals during and after low-energy electron irradiation, and seek for a conclusive interpretation of previously published and recent experimental data. The experimental observations described in Sec. II of this paper include the temperature-dependent metallization efficiency in a near-surface layer deduced from optical reflectivity data, and scanning force microscopy of irradiated surfaces revealing gas bubble formation below the surface. The observations summarized in this introduction and those described in Sec. II are discussed in Sec. III, where we develop a model for diffusion driven by electron irradiation. It is a peculiarity of low-energy electron irradiation that the development of radiation damage is strongly influenced by enhanced diffusion of charged defects in the electric field of the charge built up during electron irradiation. This effect is known in the literature as electromigration and influences for example the Auger analysis of glasses.[11] Based on our experimental findings, we propose a model for the decomposition of CaF_2 and colloid formation, in which the electric field inhibits the recombination of the primarily produced F and H centers after conversion of the H center to I and V_k centers. As a consequence of this transformation, the electric field acts as a driving force for transport of these charged defects, and especially for diffusive transport of fluorine to the surface and into the bulk of the crystal, leading to fluorine desorption at the surface and gas bubble formation in the bulk. In Sec. IV we report on the development of metallic islands at the surface. Ultrahigh-vacuum scanning force microscopy on weakly irradiated surfaces reveals the formation of 30-nm-sized atomically flat islands. We present evidence of epitaxial growth under certain experimental conditions. Another important feature of surface metal clusters is their oxidation even in an ultrahigh vacuum environment. In Sec. V, we describe the surface topographical changes that accompany such oxidation, and discuss possible mechanisms of an oxidation induced transformation of the surface cluster shape.

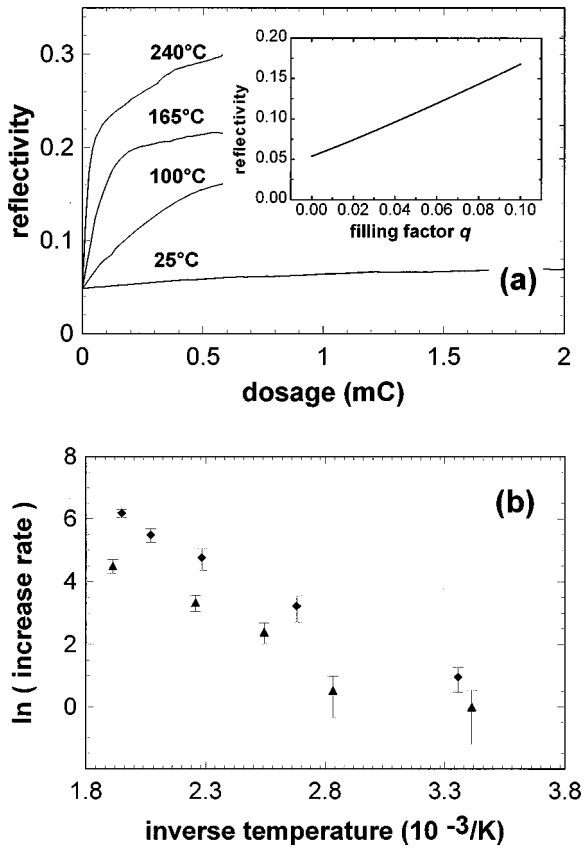

FIG. 1. (a) Development of the reflectivity of the $CaF_2(111)$ surface under electron irradiation (1 keV, 0.5 mA/cm^2) at different temperatures. The inset shows the reflectivity as a function of the fraction of Ca in CaF_2 as calculated by a theoretical model described in the text. (b) Slope of the linear increase of reflected intensity at the beginning of irradiation as a function of inverse temperature. Data sets of two different crystals are presented; the offset is a result of different probe laser intensity. Both measurements yield an activation energy for the metallization process of 0.30 ± 0.03 eV.

II. BULK DECOMPOSITION

In this section we present experimental results describing the electron-irradiation-induced decomposition of a near-surface layer. The temperature dependence of metal colloid formation efficiency is used to derive a characteristic activation energy for metal formation. Furthermore, the formation of gas bubbles during irradiation is discussed, and their depth is estimated from an elastic deformation model.

A. Temperature dependence of colloid formation

In experiments recording optical extinction spectra of colloids formed in the bulk of CaF_2 by low-energy electron irradiation, we found that colloid formation strongly depends on crystal temperature during irradiation.[8] Since a quantitative knowledge of the temperature-dependent metallization efficiency is of great importance for the understanding of the decomposition processes discussed here, we made an attempt to determine this efficiency quantitatively. Principally, this could be accomplished by an analysis of a series of colloid extinction spectra; however, we found that it is much more straightforward to extract the metallization efficiency from a measurement of sample reflectivity during the early stages of metallization. For such measurements the beam of a helium-neon laser polarized perpendicularly to the plane of incidence was reflected from the center of the electron-irradiated spot. In Fig. 1(a), the development of reflectivity as a function of irradiation time is shown at different temperatures for a sample irradiated with 0.5 mA/cm^2 of 1-keV electrons. Assuming that the reflectivity is a linear function of the amount of metal produced, the slope of the reflectivity curve in such a plot is a measure for the metal production efficiency. As expected, the reflectivity rises linearly with time in the early stages of irradiation, but levels off for longer irradiation times. While the saturation of the curves does not follow a simple function—probably due to surface metallization effects—the linear increase of reflectivity at the beginning of the irradiation at different temperatures can be used to derive the temperature dependence of the initial metallization rate. This method is based on the assumption that the reflectivity increases linearly with the volume fraction q of metallic colloids in a near surface layer for small values of q.

This has been shown for the case of spherical colloids that are small compared to the wavelength of the probing light and that do not interact with each other. For such a system with a very low density of colloids the effective dielectric constant ε_{eff} of the metallized layer can be calculated from the dielectric constants ε_{CaF_2} and ε_{Ca} of CaF_2 and Ca, respectively. Applying the Maxwell Garnet formula[12] yields

$$\frac{\varepsilon_{\text{eff}}-\varepsilon_{CaF_2}}{\varepsilon_{\text{eff}}+2\varepsilon_{CaF_2}}=q\frac{\varepsilon_{Ca}-\varepsilon_{CaF_2}}{\varepsilon_{Ca}+2\varepsilon_{CaF_2}}. \tag{1}$$

Introducing ε_{eff} into Fresnel's equations, for perpendicularly polarized light one obtains a nearly linear increase of the reflectivity from 5.4% to 10.8% when the volume fraction q rises from 0 to 5%; this curve is shown in the inset in Fig. 1(a). The volume fraction of metal produced by an electron dosage below 35 mC/cm^2, corresponding to 70-s irradiation time in Fig. 1(a), certainly does not exceed 5%, as we concluded from optical density measurements on electron-irradiated crystals not shown here. Therefore, the linear increase of the curves in Fig. 1(a) for low dosages can be identified with a linear increase of the metallized volume, and its slope can be used as a measure for the metallization rate. Figure 1(b) shows results from two different samples in an Arrhenius-type plot. The temperature range for this type of measurement is limited by the onset of calcium evaporation at temperatures above 250 °C. The slope of the curves yields an activation energy of 0.30 ± 0.03 eV for the metallization process, whereby the error is determined from results performed on different samples. An interpretation of this result will be given in Sec. III C.

B. Formation of fluorine gas bubbles

In Figs. 2(a) and 2(b), scanning force microscopy (SFM) images from two different electron-irradiated $CaF_2(111)$ surfaces are presented. The images were taken in ultrahigh vacuum using the noncontact mode[13] of a commercial scanning force microscope similar to the one introduced in Ref. 14, and Si cantilevers with a spring constant of 45 N/m, a specific conductivity of 3–5 $\Omega\,\text{cm}^{-1}$, and a resonance frequency of 300 kHz.

In Fig. 2(a), the surface is covered by islands with a lateral extension of 50 nm. These are irradiation induced calcium islands, and will be discussed in Sec. IV. Furthermore, large elevations of typically 0.5-μm diameter can be observed which are also covered by the smaller islands; the latter are interpreted as fluorine gas bubbles below the surface, yielding a surface deformation by their internal pressure. Evidence that the observed features are topographic in their nature and represent the bulged CaF_2 surface rather than any material on the surface is found in Fig. 2(b), where the elevation in the center of the image extends across two cleavage steps. Metallic islands do not appear in this micrograph, since it is differently scaled than Fig. 2(a); however, the 10-nm-high cleavage steps intersect the bubble, whereby both terraces adjacent to the step are elevated. Thus both micrographs together show that a complete CaF_2 surface layer is elevated, and these results directly visualize the decomposition of CaF_2 into fluorine gas and calcium metal.

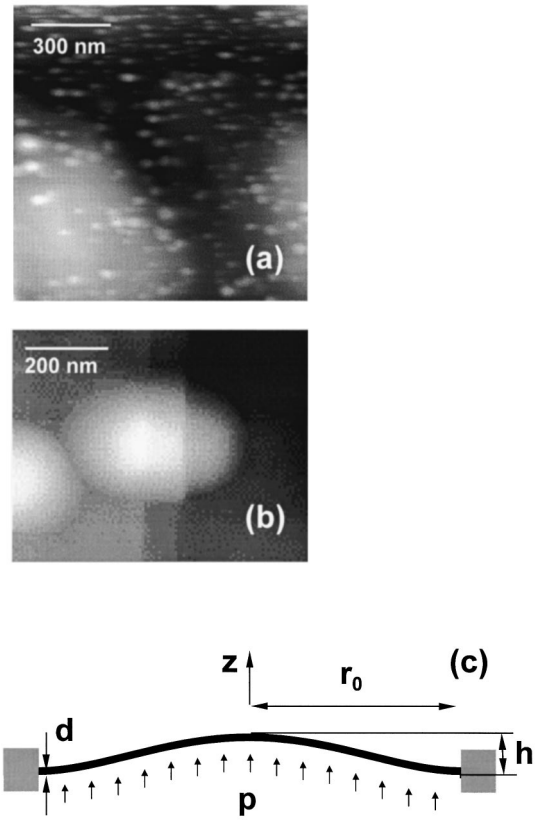

FIG. 2. (a) and (b) Scanning force micrographs of CaF_2 surfaces irradiated with 75-μA/cm^2 electrons of 850-eV energy for 10 min, at a 400-K sample temperature. The surfaces are covered by small metal islands, and partially elevated by gas bubbles formed in the bulk. (c) Schematic representation of the geometric model used to calculate the internal pressure and number of fluorine molecules in the bubble from geometric parameters derived from scanning force micrographs.

While the filling of the bubble with fluorine gas is a speculation based on our experimental evidence, this interpretation is supported by observations of Zanetti *et al.* reporting that fluorine gas bubbles evolve during ''hole drilling'' by a 100-keV electron beam in a 100-nm-thick CaF_2 layer.[2] These authors verified the presence of fluorine in the bubbles, and also its molecular character, by electron-energy-loss spectroscopy. The process of bubble formation is closely related to stimulated diffusion and will be discussed in Sec. III, while in this section we quantify the internal pressure and formation depth of the bubbles by interpreting the observed surface structure in terms of an elastic surface deformation model.

The lateral size and height of surface elevations can be used to determine the pressure of the gas and the depth of gas bubble formation following a concept introduced by Mitani and Gösele for the description of bubble formation in bonded silicon wafers.[15] The basic geometry of the problem is depicted in Fig. 2(c). This model is based on an energy minimization where the Gibbs free energy G of the bubble is the sum of the pressure energy $-pV$, the surface energy $\pi\gamma r_0^2$ for tearing apart the crystal, and the elastic energy E_{elastic} of the deformation:

$$G=-pV+\pi\gamma r_0^2+E_{\text{elastic}}. \tag{2}$$

Here p denotes the pressure in the bubble, V the bubble volume, and r_0 the radius of the bubble. The energy per unit area γ needed to separate two $CaF_2(111)$ surfaces has been determined to be 0.45 J/m^2 experimentally[16] and theoretically.[17] Assuming the elevation as a deformation of a thin circular plate fixed at its rim with a thickness d that is made from a material with an elastic modulus E and Poisson number υ, we can relate the measured geometrical properties to the internal pressure p, and find[18]

$$p = \frac{64Dh}{r_0^4} \quad \text{where} \quad D = \frac{Ed^3}{12(1-\nu)^2}. \tag{3}$$

Since Eq. (2) defines a balance between different forces acting, the equilibrium configuration can be determined by minimizing the free energy G. Further assuming ideal gas behavior for the gas in the bubble, the number of gas molecules N can be determined to be

$$N = \frac{\pi\gamma r_0^2}{\frac{3}{2}kT}. \tag{4}$$

Equation (4) states that the number of molecules in the gas bubble is determined by the relation between the energy needed to crack the crystal along a (111) plane $\pi\gamma r_0^2$ and the mean energy $\frac{3}{2}kT$ of one gas molecule inside the bubble. Within this estimate, the number of molecules in bubbles as shown in Fig. 2 is typically 10^7, with a corresponding pressure in the bubble of 5×10^7 Pa. This pressure value far above ambient air pressure explains why similar bubbles were also observable in air after removal of the irradiated samples from the UHV chamber.[10] From the pressure in the bubbles, one can calculate the thickness of the deformed layer using Eq. (3). For this thickness d of the CaF_2 layer above the bubbles, we find about 20 nm, which is of the order of the penetration depth of primary electrons for the electron energy applied here. This is the depth we expect from a model for gas collection in the bulk that is described in Sec. III.

III. ELECTRON-STIMULATED DIFFUSION

The decomposition of CaF_2 under low-energy electron irradiation involves several steps of diffusion, transformation, and aggregation of the primarily created point defects. In this section it is discussed how the diffusion of defects is influenced by the electric field resulting from electron irradiation. Therefore, in a first step the electric field built up during irradiation is described, then the development of point defects in the field is explained, and, finally, the field-enhanced diffusion of charged defects is used to explain the experimental observations described above.

A. Electric field of the charging

Charging of insulators during electron irradiation is a phenomenon that is qualitatively well understood. Generally, a layer extending into the bulk down to the penetration depth of the primary electrons will be charged negatively due to charge deposition. However, the sign of the charge at the surface is determined by an equilibrium between the fluxes of incoming primary electrons and emitted secondary electrons. For the beam geometry used in our experiments, CaF_2 has a secondary electron coefficient larger than unity in the primary electron energy range between 850 and 2500 eV relevant here;[19] i.e., for one incoming electron more than one secondary electrons leave the crystal and, therefore, the surface is charged positively during irradiation. The typical electric field resulting from such a charge distribution in an insulator irradiated by low-energy electrons has been described by Cazaux,[11] and is schematically drawn in Fig. 3(a). Note that there are two inversion points where the electric field changes its sign. The first one is very close to the surface, and not relevant for the following discussion. In this field configuration, negatively charged defects created between the two inversion points are driven toward the surface, while those created beyond $P_{\mathrm{inv},2}$ are driven further into the bulk. Quantitative estimates for the electric field are difficult to obtain since the energy distribution of secondary electrons as well as the conductivity of the crystal under irradiation are not known. However, the apparent positive surface potential can be estimated from measurements of the kinetic energy of positive ions desorbing during electron irradiation.[7] As a consequence of the described charging profile, charged defects experience a strong electric field in the surface layer and are driven toward the surface or into the bulk depending on the sign of their charge and their position with respect to the inversion points of the profile. Thus the main driving force for diffusion is the electric field rather than thermal activation.

B. Development of defects under low-energy electron irradiation

The primary localized excitation in CaF_2 due to electron irradiation is the self-trapped exciton (STE).[20] This metastable defect may relax into the regular lattice, but may also separate into a pair of an F center (an electron trapped at an anion vacancy) and an H center (a fluorine atom at an interstitial site covalently bound to a lattice anion); however, the probability of such a separation is extremely low for CaF_2 if energy is only provided by thermal excitation at crystal temperatures discussed here.[21] It has been shown, however, that the separation can be induced by excitation of the hole center of the STE with 5-eV photons[22] but the lifetime of separated F-H pairs in CaF_2 is limited to milliseconds due to recombination.[21] We propose that in our case of low-energy electron excitation secondary electrons provide the hole center excitation, and this is the primary source of F and H center defects leading to metallization.

Since only stable F centers may aggregate into metallic colloids, there must be a mechanism inhibiting recombination. As a second basic assumption we propose that this inhibition is accomplished by separating the H center into a pair of an I center (anion at an interstitial site) and a V_k center (hole binding two anions to a F_2^- molecule). Such a defect transformation is thermodynamically favored[23] and may be enhanced by the hole excitation mechanism described above. The end product of the transformation are charged species, namely, V_k centers and I centers that are separated in the electric field due to their opposite charge.

Since the V_k center has a rather high mobility,[24] it is readily taken away and neutralized by an excess negative charge in the bulk and recombination with a F center is effectively inhibited. This has to be seen in contrast to radiolysis experiments involving high-energy photons where internal electric fields do not play an important role. In this case V_k centers simply annihilate F centers when measuring at temperatures where the holes are mobile. For the interpretation of such experiments it has been shown, however, that various complexes of I center and F center defects are stable.[23] Therefore, it is also reasonable to assume a coexistence of these species in our case. In summary, the electron-irradiation-induced electric field is found to be prerequisite for the formation of stable F centers and I centers that are the primary source of the metallization discussed here.

C. Field-enhanced defect diffusion

In this scenario the irradiation induced electric field is the driving force for fluorine mass transport as well as charge transport in the form of V_k centers. A similar mechanism described as electric-field assisted diffusion of fluorine ions was introduced by Ibara *et al.*[25] for the explanation of the temporal development of the yield of electron stimulated desorption from CaF_2. The diffusion of these species illustrated in Fig. 3(b) is determined by the profile of the electric field sketched in Fig. 3(a). While V_k centers are collected at the inversion point $P_{\mathrm{inv},2}$, I centers are driven towards the surface or into the bulk depending on whether they are created above or below $P_{\mathrm{inv},2}$. V_k centers collected at $P_{\mathrm{inv},2}$ may capture excess electrons in this negatively charged region, recombine, and provide partial charge neutralization in the bulk.

The activation energy of 0.3 eV found in Sec. II for this metallization process matches the well-known activation energy for V_k center diffusion.[26] The mobility μ of V_k centers in an electric field is related to their diffusivity D by the Einstein relation $D=\mu kT$. Although the relation between D and μ is scaling with the temperature T, in the temperature range used in these experiments the temperature dependence of both μ and D are dominated by a Boltzmann factor with the activation energy of about 0.3 eV. Therefore, the activation energies of μ and D can be compared directly. The correspondence of the temperature dependence of metallization and V_k center diffusion supports the assumption of our model that the diffusion of V_k centers is the essential first step for the development of stable defects and subsequent metallization in CaF_2 under low-energy electron irradiation. Much higher values would be expected for the activation of the diffusion of F and I centers, at least in their ground state.[26,27]

I centers driven toward the surface are the major source for the strong delayed desorption of fluorine observed during electron irradiation. Reaching the surface they replace desorbed fluorine and this substitution mechanism explains the temporal development of the fluorine desorption demonstrated in Ref. 9. The desorption reaches a maximum when fluorine from the inversion point $P_{\mathrm{inv},2}$ reaches the surface and subsequently decreases due to the fluorine depletion in the penetration range of the electrons. The increase of the desorption yield is due to the two times higher excitation

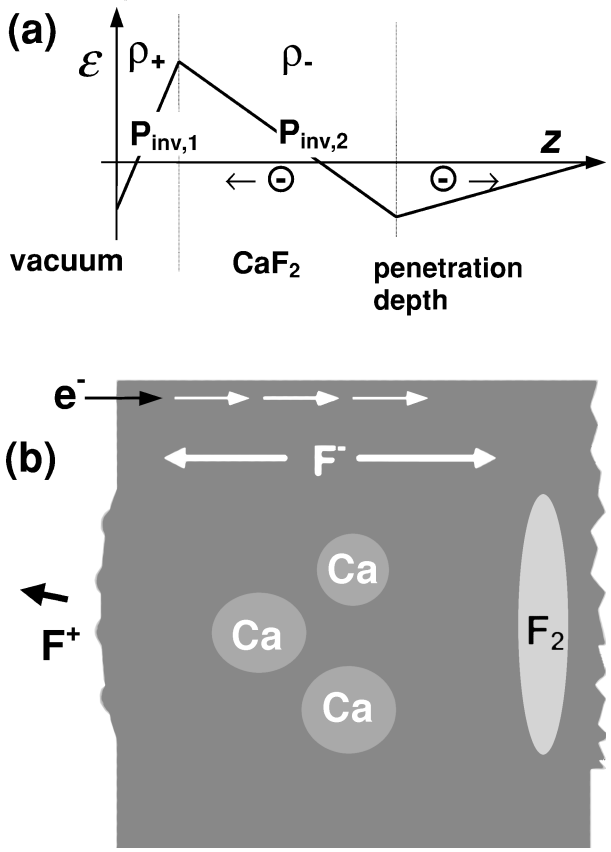

FIG. 3. Schematic representation of the model for the decomposition of CaF_2 under low-energy electron irradiation. (a) Electric field ε vs depth z. The field strength is determined by the negative charge ρ_- in the bulk and the positive charge ρ_+ at the surface due to secondary electron emission (after Ref. 11). The field direction is inverted at points $P_{\mathrm{inv},1}$ and $P_{\mathrm{inv},2}$. (b) Electron-irradiation-induced processes: Transport of fluorine ions to the surface and into the bulk and fluorine desorption. Calcium colloids develop at the surface and in the bulk while, fluorine gas bubbles are formed slightly below the inversion point $P_{\mathrm{inv},2}$.

density at $P_{\mathrm{inv},2}$ compared to that at the surface.[7] I centers driven into the bulk yield a fluorine enrichment in a depth somewhat larger than the penetration depth of the electrons. Here the fluorine gas bubbles described in Sec. II are formed. The depth of the bubbles of 20 nm estimated in Sec. II C is well in agreement with the expectation depicted in Fig. 3(b) that the electric field driving the fluorine ions into the bulk reaches beyond the penetration depth of the primary electrons that is 15 nm for 850-eV electrons. Calculating the number of fluorine molecules stored in the bubbles shown in Fig. 2 according to the estimates of fluorine production presented in Sec. II B, we find that about two triple layers of CaF_2 are dissolved in the bubbles in what appears to be a plausible number with regard to the remaining stability of the crystal.

The last step in this process is the formation of metallic bulk and surface clusters. In the bulk this is straightforward since fluorine is removed and the remaining metal ions readily form precipitates with a size and shape determined by the random action of initial defect formation. We assume that most of the colloids grow around the inversion point $P_{\mathrm{inv},2}$, where field-enhanced diffusion causes a fluorine

depletion leaving behind vacancies that may capture excess electrons to form *F* centers. When providing enough thermal energy, *F* centers become mobile, and little diffusion is required to form regular metallic colloids observed at elevated temperatures.[8]

However, diffusion rather than fluorine desorption has been found to be the driving force for surface metallization in low-intensity electron-irradiation experiments.[10] There the integrated volume of metal islands on the CaF_2 surface produced by electron irradiation was found to grow quadratically with the applied irradiation time, which can be explained by assuming that the surface metallization is built up by diffusion of *F* centers from the bulk to the surface but diffusive transport is restricted to the duration of electron irradiation. The latter assumption can now be understood in the framework of the model depicted above. *F* centers are created and stabilized as long as there is an electron-irradiation-induced electric field; however, as soon as the irradiation is switched off both the creation of charged species as well as their field driven diffusion will stop immediately. Any remaining defects will recombine with their complements since there is no separating force anymore. Thermally stimulated diffusion experiments have shown that above 270 K *F* centers are mobile enough to aggregate into metallic colloids of up to 25-nm radius.[8] Furthermore, during irradiation the *F* centers may be excited and therefore possess a lowered activation energy for diffusion. Temporarily *F* centers may even be ionized, forming vacancies which are then driven by the electric field toward the inversion point $P_{\mathrm{inv},2}$. All these excitation processes could enhance the efficiency of colloid formation.

IV. SURFACE METALLIZATION

As we know that surface metallization due to electron irradiation at elevated temperatures is to a large extent fed by *F* center diffusion from the bulk, it is interesting to investigate the ordering of metal on the surface in some detail. Here we focus on irradiations that are weak compared to those applied in earlier studies[10]; i.e., we irradiated crystals at a temperature of typically 400 K with an average current density of 5 $\mu A/cm^2$ of 850-eV electrons for 10 min. After cooling crystals to room temperature they were inspected by scanning force microscopy in the non-contact mode where a bias voltage was applied to the rear side of the sample to minimize electrostatic forces.[28] Since the electron beam does not have a flat intensity profile and the SFM samples only a very small fraction of the irradiated area that cannot be well located within the spot, the dosage density relevant for a specific SFM micrograph is not known precisely and the irradiation parameters given define an upper limit.

Figure 4 shows a typical micrograph obtained in this way where surface elevation is coded in the form of a false color representation. The most obvious features in this micrograph are five terraces descending from the lower left to the upper right corner. Terraces are separated by steps with a height of 0.32 nm corresponding to the distance between (111) triple layers in the CaF_2 structure. The color scaling has been chosen so that the level of each of the terraces corresponds to one of the main colors yellow, green, cyan, blue, and red. Terraces are covered by randomly distributed islands of 20–30 nm lateral extension. Closer inspection of the colors of the islands reveals that all of them exhibit the color of the next higher or next but one higher terrace, respectively. Therefore, most islands are formed by two layers of the same height as the step height between CaF_2 terraces. This observation is in accordance with our expectation of an epitaxial growth during the initial steps of metallization. The distance between (111) planes in metallic calcium equals the distance between (111) triple layers in the CaF_2 structure due to the matching lattice structures of CaF_2 and metallic Ca and due to their nearly equal lattice constants, as can be seen in the compilation of data in Table I. While this observation reveals a growth in ordered layers we sometimes also observe ordering phenomena in lateral directions. Most islands exhibit a rather irregular contour; however, in some cases we find clearly triangular shapes, as demonstrated in the upper right of Fig. 5, representing a magnified section of the same surface as in Fig. 4. Again, the islands consist of two layers where the upper layer resembles the symmetry of the (111) surface by its triangular shape. This type of ordering is only observed for a range of crystal temperatures providing a certain level of surface mobility during colloid formation. The triangular shape is most probably a result of energy minimization, forcing the colloid into a shape with a minimum number of low-coordinated sites, while at the same time allowing epitaxy in island formation that is fostered by a strong interaction of the metallic cluster with the underlying substrate. The detailed mechanisms of formation of islands of such shapes will be described in a forthcoming paper.

It is interesting to relate our results to experiments of silicon growth on electron-irradiated CaF_2 reported by Petterson, Miles, and McGill.[6] These authors found that the roughness of Si films grown on CaF_2 can be reduced by preirradiation with low-energy electrons. The best results have been found for irradiation conditions comparable to those used for the preparation of the surface shown in Fig. 4. The atomically flat metal islands provide a higher free surface energy compared to CaF_2 which is needed to enforce a two dimensional growth of the silicon film. The need of a direct Si-Ca bond at the CaF_2/Si interface for smooth film growth has also been shown for the reversal growth of CaF_2 on Si.[29]

V. OXIDATION OF SURFACE CLUSTERS

In a previous paper,[28] we showed preliminary results on SFM imaging of irradiated surfaces inspected a long time after irradiation. In such micrographs we found peculiar surface features, namely, holes and adjacent elevations, that cannot be explained by ordering processes discussed in Sec. IV. We tentatively assigned the observed phenomena either to a true topographic structure developing with time or artifacts due to local charge accumulation. Here we revisit this phenomenon, present results from more systematic studies, and aim for a conclusive interpretation of such SFM micrographs. We are now convinced that they represent true topographic features resulting from a structural transformation of surface metal clusters during oxidation or hydroxylation in the residual gas atmosphere, and are not related to charging.

Our discussion here is based on a series of micrographs obtained from irradiated surfaces where the time elapsed be-

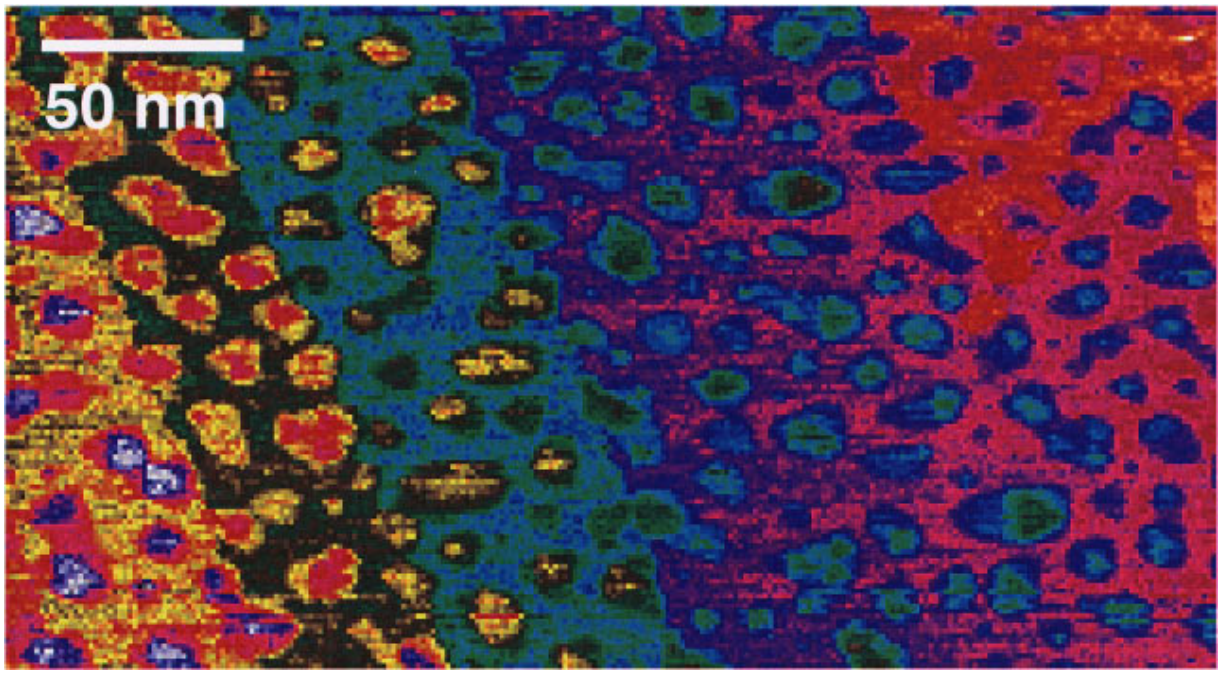

FIG. 4. (Color) Surface metallization after weak electron irradiation (5 μA/cm^2, 10 min, 850 eV, 410 K). The false color representation shows five terraces descending from the lower left to the upper right corner. The irradiation-induced metal islands exhibit colors of the next higher terraces.

tween irradiation and SFM imaging was systematically varied between 6 and 40 h; the respective scanning results are displayed in Figs. 6(a)–6(d). The topography in frame (a) representing 6-h waiting time is very similar to that of Fig. 4, i.e., the terraced surface is randomly covered by surface clusters of 1-ML height and nanometers lateral extension frequently topped by a second monatomic layer of smaller lateral extension. Areas between clusters are atomically flat within the precision of the measurement. First stages of a transformation can be recognized in frame (b), taken 16 h after irradiation. While the basic structure of surface colloids is still preserved, there appear small holes adjacent to most of the clusters. Although their lateral extension is only a few nanometers and the tip cannot precisely replicate the structure of the holes, to our knowledge they are a distinctly new feature with a depth of at least 0.5 nm. Frame (c), representing a result for 24-h waiting time, shows the next step in this progression where the visible hole area has considerably

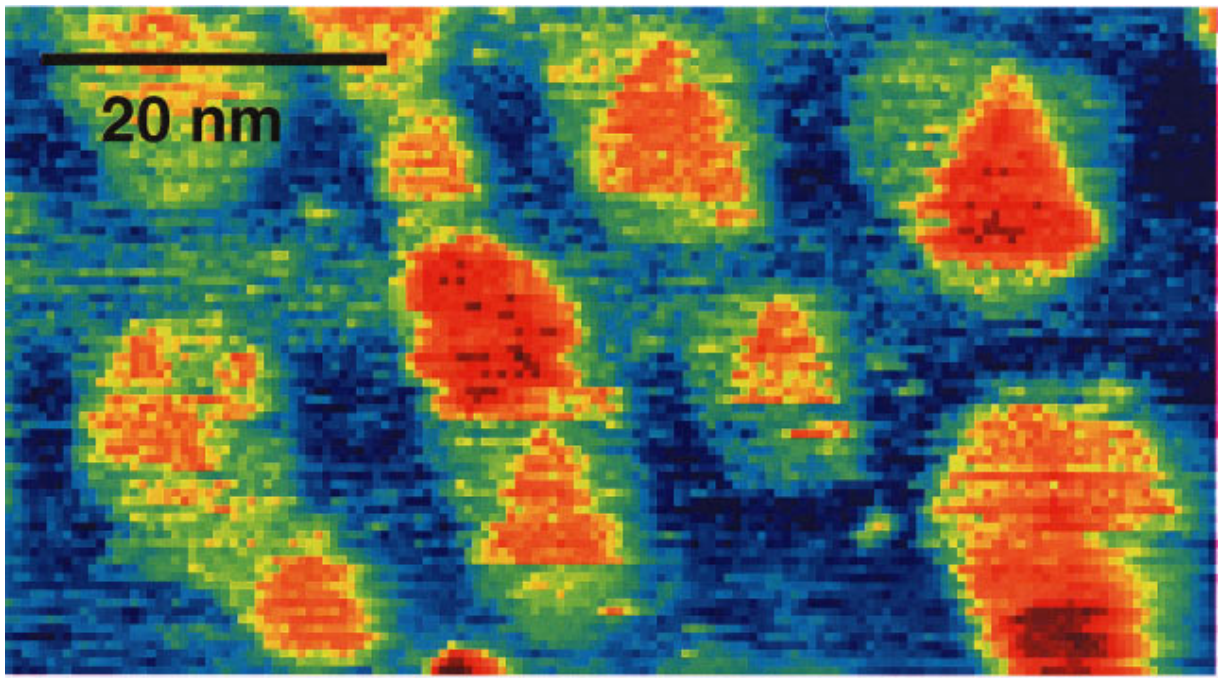

FIG. 5. (Color) Magnified area from the same surface as in Fig. 4, demonstrating the alignment of surface metal clusters along the symmetry lines of the (111) surface.

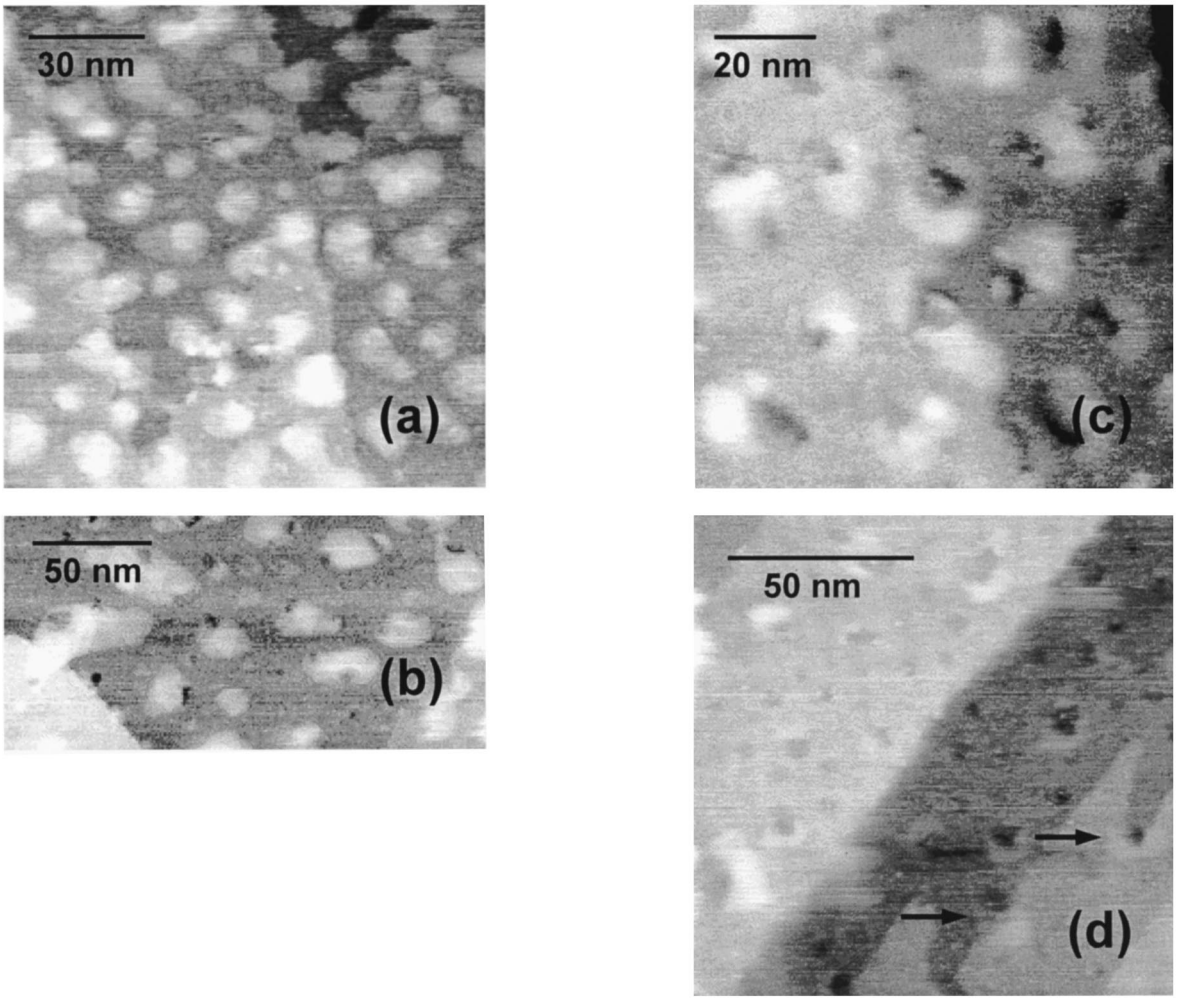

FIG. 6. Surface metal cluster formation and oxidation on various surfaces observed as a function of waiting time elapsed between irradiation and SFM imaging. (a) Micrograph taken 6 h after 600-s irradiation at 410 K. (b) Micrograph taken 16 h after 120-s irradiation at 343 K. (c) Micrograph taken 24 h after 600-s irradiation at 410 K [same surface and irradiation as frame (a)]. (d) Micrograph taken 40 h after 120-s irradiation at 385 K.

grown compared to the previous frame, and in some cases the metal exhibits a tendency of surrounding the hole in a ringlike structure. Note that the metal clusters now have a shape significantly differing from that found in frame (a). The tendency of a structural transformation is even more evident in the final frame (d), representing results obtained 40 h after irradiation. The most striking feature evident in this frame, however, is the accumulation of metal on top of cleavage steps or tips, where the corresponding hole is located at the adjacent lower terrace [see the arrows in frame (d)]. We have not observed any significant further transformation for waiting times longer than one 40 h.

The surface topography is markedly different when the substrate temperature during irradiation is significantly above 400 K; a typical example for an irradiation at 445 K is shown in Fig. 7. In this SFM micrograph we do not observe traces of surface colloids, but a strong surface erosion manifest in irregularly shaped holes covering the surface. This surface structure is reminiscent of SFM micrographs taken in air on crystals irradiated at lower temperature, where the surface metal has been removed by exposure of the surface to water.[10] As in this previous case, we interpret the holes as locations of preferential surface erosion similar to the holes observed in micrographs from Fig. 6 found at lower temperature. In contrast to these lower-temperature measurements, in the experiment shown in Fig. 7, surface metal has evaporated from the surface leaving behind the eroded CaF_2 surface. The high density of holes is testament to the strong enhancement of erosion when the temperature is raised (see Sec. II), since the irradiation time in this experiment was rather small compared to other measurements presented before.

In an effort at a conclusive interpretation of the experimental evidence compiled in the previous paragraph, we first collect arguments ruling out that the observed features are due to surface charging effects. This is not *a priori* evident, since noncontact SFM imaging is as equally susceptible to surface topography as charging, and there is no inherent way of discrimination between these effects when judging a micrograph.[30] Furthermore, the holes detected in the surface principally provide a plausible explanation for charging artifacts, since they are defects that might accumulate charged defects. Our main argument for dismissing charging as an origin of the features observed in the series of Fig. 6 is the fact that transformation effects progressively develop as a function of waiting time after irradiation, while charging effects would decay. The latter has been verified in numerous

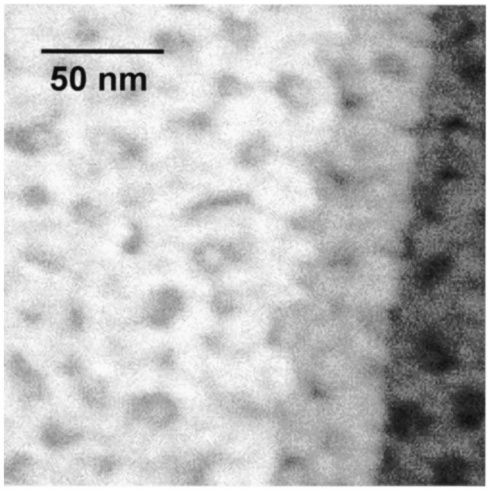

FIG. 7. Crater formation on a surface irradiated at higher temperature. The SFM micrograph was taken 16 h after 40-s irradiation at 445 K.

experiments on freshly cleaved surfaces, where any surface charge initially present did decay with waiting time, and charging reached a level insignificantly influencing SFM imaging after a few days. Freshly cleaved surfaces certainly contain many defects with a potential of charge accumulation; however, we never observed a local increase in charging nor did we find evidence of charging due to an external electron source like the filament of the ion gauge in the vacuum system. Of course, electron irradiation introduces a considerable amount of charge, but this charge will decay with time due to the ionic conductivity of the CaF_2 crystal.[28] Hence the only possible mechanism yielding local charging increasing with time would be a concentration resulting from diffusion and trapping at defects. However, we know that such diffusion is strongly enhanced by temperature, and by moderate heating (470 K) of a CaF_2 crystal it is, for example, possible to completely eliminate surface charging during photoemission experiments.[31] Hence the major contribution to a possible charge concentration would be expected immediately after electron irradiation when the crystal is still hot, and a concentration effect should be visible soon after irradiation and will not develop during days where the crystal is kept at room temperature. In view of all these results and conclusions, it appears to be highly improbable that charging plays any role in the time development found in SFM micrographs presented above.

To explain the surface structural transformations evident in Fig. 6, we instead suggest a model based on the assumption that the metallic surface colloids progressively oxidize during exposure to the residual gas atmosphere in the ultrahigh-vacuum apparatus. In previous papers we showed by x-ray photoelectron spectroscopy that such oxidation occurs for surface clusters that had been prepared similarly to those discussed here, and that the oxidation in the ultrahigh-vacuum environment occurs on a time scale of some ten hours, very compatible with what we observe here.[10,32] More recently we investigated band-gap electronic states emerging after a controlled dosage of the CaF_2 surface with various gases using ultraviolet photoelectron spectroscopy, and found that the electron irradiated surface is readily oxidized or hydroxilized by oxygen and water, while dosing with nitrogen and carbon dioxide did not yield a measurable effect.[33] Based on the latter results we anticipate that oxygen and water are the main components of the residual gas responsible for the structural changes observed in the SFM measurements presented here. Within this model the process of surface erosion, colloid formation, and transformation can be described as occurring in several steps. The primary step is a preferential erosion at sites randomly distributed over the surface, although we presently do not know details about these sites. Apparently the holes observed in SFM micrographs are the main source of surface metal, and we speculate that they represent the end points of channels supplying metal by pipe diffusion. Initially the holes are covered by metal, and material emerging from below the holes is distributed over the adjacent surface, thus forming surface clusters with a height not larger than two monolayers. If the irradiation is stopped at this point where the average surface coverage is about one monolayer and the temperature is decreased, the initially formed clusters are stabilized, and the surface structure does not change significantly during several hours. However, prolonged exposure to the residual gas leads to progressive oxidation of the clusters. As can be seen in Table I, lattice structure and interionic spacing in Ca and CaO, and consequently the respective specific volumes, do not match well. Therefore, during the time of oxide formation there will also be a buildup of surface stress in the cluster exerting forces on the parts deeper in the holes. To minimize its surface energy, the oxidizing cluster undergoes a transformation from the originally flat platelet with some extension into the hole to a more spherical shape. Internal adhesive forces yield a removal of material from the hole into the cluster adjacent to the hole. The transformation is supported by progressive oxidation weakening the adhesion between the cluster and the CaF_2 surface.

VI. SUMMARY

Irradiation of CaF_2 with low-energy electrons results in bulk and surface metallization as well as fluorine desorption. We demonstrated that these processes are closely related to each other, and that bulk and surface readily communicate with each other by diffusion of charged defects. A major conclusion from various pieces of experimental evidence is that this diffusion is not only thermally activated but mainly driven by the electric field built up in a surface layer of the crystal during electron irradiation. We presented a model proposing that, in a highly excited surface layer, self-trapped excitons as the primary product of electron irradiation to some extent are converted into I center and V_k center defects. I centers are then driven to the surface feeding fluorine desorption but also into the bulk where the formation of fluorine gas bubbles is observed, while V_k centers provide charge neutralization in a depth corresponding to the penetration depth of the primary electrons. This mechanism of fluorine depletion fosters the formation of metal colloids even at low temperature where only V_k centers are mobile.

The investigation of the topography of electron-irradiated surfaces yields evidence of strongly inhomogeneous surface erosion. In the initial stages of surface metallization, well-

ordered nanometer-sized precipitates of 1–2-ML height are formed. Under certain experimental conditions the epitaxial growth in lateral direction is influenced by the substrate in a way producing triangular surface clusters reproducing the substrate surface symmetry. The topography drastically changes upon exposure of the surface to the residual gas atmosphere during several days. The initially well-ordered, flat precipitates are transformed into more irregularly shaped three-dimensional clusters found at the edges of surface holes which were previously covered by the clusters. We documented several stages of this transformation, and proposed that this process is induced and maintained by progressive oxidation of metallic clusters in the residual gas atmosphere.

ACKNOWLEDGMENTS

The authors are grateful to E. Matthias for important contributions and continued support of this work. Stimulating discussions with R. T. Williams and A. Popov and experimental assistance by R. M. Wilson and M. Huisinga are gratefully acknowledged. This work was supported by the Sonderforschungsbereich 337 of the Deutsche Forschungsgemeinschaft.

*Present address: University of Basel, Department of Physics and Astronomy, Klingelbergstr. 82, 4056 Basel, Switzerland.

†Corresponding author. Electronic address: reichling@physik.fu-berlin.de

[1] Y. Hirose, S. Horng, A. Kahn, C. Wrenn, and R. Pfeffer, J. Vac. Sci. Technol. A **10**, 960 (1992).

[2] R. Zanetti, A. L. Bleloch, M. P. Grimshaw, and G. A. C. Jones, Philos. Mag. Lett. **69**, 285 (1994).

[3] T. Suemasu, Watanabe, J. Suzuki, Y. Kohno, M. Asada, and N. Suzuki, Jpn. J. Appl. Phys. **33**, 57 (1994).

[4] A. Izumi, K. Tsutsui, and S. Furukawa, J. Appl. Phys. **75**, 2307 (1994).

[5] K. Kawasaki and K. Tsutsui, Appl. Surf. Sci. **117/118**, 753 (1997).

[6] P. O. Pettersson, R. J. Miles, and T. C. McGill, J. Appl. Phys. **76**, 7328 (1994).

[7] R. Bennewitz, D. Smith, M. Reichling, E. Matthias, N. Itoh, and R. M. Wilson, Nucl. Instrum. Methods Phys. Res. B **101**, 118 (1995).

[8] R. Bennewitz, C. Günther, M. Reichling, E. Matthias, S. Vijayalakshmi, A. V. Barnes, and N. H. Tolk, Appl. Phys. Lett. **66**, 320 (1995).

[9] M. Reichling, Nucl. Instrum. Methods Phys. Res. B **101**, 108 (1995).

[10] M. Reichling, R. M. Wilson, R. Bennewitz, R. T. Williams, S. Gogoll, E. Stenzel, and E. Matthias, Surf. Sci. **366**, 531 (1996).

[11] J. Cazaux, J. Appl. Phys. **59**, 1418 (1986).

[12] W. Theiß, in *Festkörperprobleme*, edited by R. Helbig (Vieweg Braunschweig, Wiesbaden, 1994), Vol. 33, p. 149.

[13] T. R. Albrecht, P. Grütter, P. Horne, and D. Rugar, J. Appl. Phys. **69**, 668 (1991).

[14] L. Howald, E. Meyer, R. Lüthi, H. Haefke, R. Overney, H. Rudin, and H.-J. Güntherodt, Appl. Phys. Lett. **63**, 117 (1993).

[15] K. Mitani and U. M. Gösele, Appl. Phys. A **54**, 543 (1992).

[16] J. J. Gilman, J. Appl. Phys. **31**, 2208 (1960).

[17] P. W. Tasker, J. Phys. C **6**, 488 (1980).

[18] H. Leipholz, *Theory of Elasticity* (Nordhoff, Leyden, 1974).

[19] L. Reimer, *Image Formation in Low-Voltage Scanning Electron Microscopy*, Tutorial Texts in Optical Engineering Vol. TT12 (SPIE, Bellingham, WA, 1993).

[20] K. S. Song and R. T. Williams, *Self-Trapped Excitons*, Springer Series in Solid-State Science Vol. 105 (Springer-Verlag, Berlin, 1993).

[21] L. A. Lisitsyna, V. M. Lisitsyn, and E. P. Chinkov, Russ. Phys. J. **38**, 9 (1995).

[22] K. Tanimura, T. Katoh, and N. Itoh, Phys. Rev. B **40**, 1282 (1989).

[23] C. R. A. Catlow, J. Phys. C **12**, 969 (1979).

[24] W. Hayes, *Crystals with the Fluorite Structure* (Oxford University Press, London, 1974).

[25] O. Ibara, J. Cazaux, G. Remond, and C. Gilles, J. Appl. Phys. **79**, 2309 (1996).

[26] K. Atobe, J. Chem. Phys. **71**, 2588 (1979).

[27] J. W. Twidell, J. Phys. Chem. Solids **31**, 299 (1971).

[28] R. Bennewitz, M. Reichling, and E. Matthias, Surf. Sci. **387**, 69 (1997).

[29] J. D. Denlinger, E. Rotenberg, U. Hessinger, M. Leskovar, and M. A. Olmstead, Phys. Rev. B **51**, 5352 (1995).

[30] J. E. Stern, B. D. Terris, H. J. Mamin, and D. Rugar, Appl. Phys. Lett. **53**, 2717 (1988).

[31] M. Huisinga, M. Reichling, and E. Matthias, Phys. Rev. B **55**, 7600 (1997).

[32] M. Reichling, M. Huisinga, D. Ochs, and V. Kempter, Surf. Sci. **402–404**, 145 (1998).

[33] M. Huisinga, V. E. Puchin, and M. Reichling, Nucl. Instrum. Methods Phys. Res. B **141**, 528 (1998).